The role of mitochondria linked fatty-acid uptake-driven adipogenesis in Graves' Orbitopathy

Lei Zhang[1], Pavandeep Rai[3], Satomi Miwa[4], Mohd Shazli Draman[1], D. Aled Rees[1], Anjana S Haridas[2], Daniel S Morris[2], Andrew R Tee[1], Marian Ludgate[1], Doug M Turnbull[3] & Colin M Dayan[1]

[1] School of Medicine, Cardiff University, Heath Park, Cardiff, CF14 4XN, U.K.

[2] Department of Ophthalmology, Cardiff & Vale University Health Board, Heath Park, Cardiff CF14 4XW, U.K.

[3] Wellcome Centre for Mitochondrial Research, Translational and Clinical Research Institute, Faculty of Medical Sciences, Newcastle University, Newcastle, NE2 4HH, U.K.

[4] Biosciences Institute, Newcastle University, Newcastle Upon Tyne, NE4 5PL, U.K.

Short title: The essential role of mitochondria in Graves' Orbitopathy

Key words: Graves' Orbitopathy; Orbital Adipose Tissue; fatty acid uptake; adipogenesis; mitochondria OXPHOS; ATP production.

Address correspondence to: Lei Zhang, Research Fellow in School of Medicine, Cardiff University, Heath Park, Cardiff, CF14 4XN, U.K. Tel. (44)2920742343, Fax. (44)2920744671, email: zhangL14@cf.ac.uk

Grants: This research did not receive any specific grant from funding agencies.

Disclosure Statement: The authors have nothing to disclose.

Abstract

Context

Depot-specific expansion of orbital-adipose-tissue (OAT) in Graves' Orbitopathy (GO, an autoimmune condition producing proptosis, visual impairment and reduced quality of life) is associated with fatty-acid (FA) uptake-driven adipogenesis in preadipocytes/fibroblasts (PFs).

Objective

A role for mitochondria in OAT-adipogenesis in GO.

Design/Setting/Participants

Confluent PFs from healthy OAT (OAT-H), OAT from GO (OAT-GO) and white-adipose-tissue in culture-medium compared with culture-medium containing a mixed hormonal-cocktail as adipogenic-medium (ADM); or culture-medium containing FA-supplementation, oleate:palmitate:linoleate (45:30:25%) with/without different concentration of mitochondrial bio-substrate ADP/GDP, AICAR (adenosine-analog) or inhibitor oligomycin-A for 17 days.

Main outcome measures

Oil-Red-O staining and foci-count of differentiated adipocytes for in-vitro adipogenesis; flow-cytometry, relative-QPCR, MTS-assay/10^6 cells, total cellular-ATP detection kit and Seahorse-XFe96-Analyzer for mitochondria and OXPHOS/Glycolysis-ATP production analysis.

Results

During early adipogenesis before adipocyte formation (day-0,4&7), we observed OAT-specific cellular ATP-production via mitochondrial-OXPHOS in PFs from both OAT-H/OAT-GO, and substantially disrupted OXPHOS-ATP/Glycolysis-ATP production in PFs from OAT-GO, e.g. 40% reduction in OXPHOS-ATP and trend-

increased Glycolysis-ATP production on day-4&7 compared with day-0, which contrasted with the stable levels in OAT-H.

FA-supplementation in culture-medium triggered adipogenesis in PFs from both OAT-H/OAT-GO, which was substantially enhanced by 1mM GDP reaching 7-18% of ADM-adipogenesis. The FA-uptake-driven adipogenesis was diminished by oligomycin-A but unaffected by treatment with ADP or AICAR. Furthermore, we observed significant positive correlation between FA-uptake-driven adipogenesis by GDP and the ratios of OXPHOS-ATP/Glycolysis-ATP through adipogenesis of PFs from OAT-GO.

Conclusions

Our study confirmed that FA-uptake can drive OAT-adipogenesis and revealed a fundamental role for mitochondria-OXPHOS in GO development, which provides potential for therapeutic interventions.

Introduction

Graves' Orbitopathy (GO), also called thyroid eye disease, is a disfiguring disease of the orbit with a higher incidence in women (80%) (1,2). The uncontrolled expansion of orbital adipose tissue (OAT) contributes to proptosis, double vision and in some cases visual loss. GO develops mainly in the context of an autoimmune condition, Graves' disease, in which thyrotropin receptor (TSHR) activation by thyroid stimulating antibodies (TSAB) mimics the action of TSH producing hyperthyroidism (1,2). The TSHR is also detected and increased in OAT in GO, and is an essential cellular target for both GO and Graves' disease (3-6). Previous GO studies have examined the cross-talk of signalling pathways via two cell-surface receptors, TSHR and insulin like growth factor 1 receptor (IGF1R), focusing on disease targeted preadipocytes/fibroblasts (PFs) embedded in OAT (7,8).

OAT-PFs are mesenchymal stem cell (MSC) with multi-differentiation potentials, as has been described by ourselves and others (9-11). In GO patients, the excessive adipogenesis via lineage-specific differentiation of PFs in OAT occurs rapidly (1,12). By contrast, WAT (white adipose tissues) from the same individual typically shrinks in Graves' disease due to hyperthyroidism (2). Previously we described a cell specific signalling network (PI3K/Akt/mTORC1/FOXOs) in PFs from human OAT not present in WAT (13,14). The identified pathways interact with TSHR/IGF1R signalling to play essential roles in the depot-specific OAT expansion in GO (2). Our recent work has demonstrated that OAT is a distinctive metabolic-quiescent fat depot which neither stores additional triglyceride in obesity (15) nor burns fatty acid (FA) (11), in contrast to WAT and BAT (brown adipose tissue)/BRITE (BRown in whITE), respectively. OAT also displays a unique FA-uptake-driven adipogenesis mechanism, which occurs in addition to the hyperplastic expansion (increased adipocyte number) of PFs in OAT

88 in GO (11). In particular, lower lipolytic activity with similar (low) FA-synthesis
89 accompanied by increased expression of a depot-specific FA-transporter (SLC27A6)
90 were observed in OAT from healthy individuals (OAT-H) and GO patients (OAT-GO)
91 compared with WAT (11).
92 Involvement of mitochondrial dysfunction in the orbital fat expansion in GO is
93 suggested by increased expression of the uncoupling protein UCP1 in OAT from GO.
94 This has been observed both in human models - ex-vivo analysis of OAT-GO (11),
95 GO-targeted PFs by TSHR activation (16,17) - and a mouse model of TSHR-induced
96 GO (18). UCP1 expression in mitochondria is a known feature of BAT, which dissipates
97 energy as heat by uncoupling mitochondrial oxidative-phosphorylation (OXPHOS) from
98 ATP production and also plays an important role in mitochondrial function (19).
99 Hyperplastic expansion of adipocytes in human BAT caused by mitochondrial
100 dysfunction via mutation of *MFN2* has recently been reported (20). Substantially
101 increased expression of *MFN2* has also been observed in OAT from GO patients
102 compared with OAT-H in our recent study (11). Overexpression of adiponectin which is
103 also a mitochondrial function modulator has been shown to induce expansion of both
104 OAT and BAT in a mouse model (21,22).
105 These factors, together with the identified specific molecular signatures of OAT (e.g.
106 Sirtuin/Wnt/Ca+ signaling pathways) from our recent study suggest a role for
107 mitochondria in the development of GO (11). Apart from being a cellular 'power-
108 house', mitochondrial-OXPHOS and its bio-substrates, e.g. ATP/ADP, GTP/GDP,
109 play fundamental roles in the regulation of cell metabolism through interacting with
110 complex molecular cascades, e.g. cell proliferation, differentiation (23,24).
111 Our current study investigated the hypothesis that dysfunction of mitochondria plays a
112 role in the FA-uptake-driven adipogenesis in OAT expansion in GO. Our investigation

demonstrated mitochondrial dysfunction in PFs from OAT-GO, which linked with the confirmed FA-uptake-driven adipogenesis from in vitro adipogenesis analysis.

Materials and Methods

All reagents were obtained from Sigma-Aldrich (U.K.) and tissue culture components from Cambrex (U.K.) unless otherwise stated.

Adipose Tissue Collection & Preparation

Adipose Tissue was collected with informed written consent and local research ethics committee approval. WAT (subcutaneous) was from 10 patients undergoing elective open abdominal or breast surgery for non-metabolic conditions. OAT from GO patients (n=13) were from 10 inactive GO patients with a CAS (clinical activity score)<2, 3 active GO patients with CAS≥3 undergoing 2-wall or 3-wall orbital decompression surgery. Most of the GO patients had carbimazole treatment, RAI and/or thyroidectomy in the past; two GO patients received no anti-thyroid treatment and two were receiving carbimazole treatment while the OAT samples were obtained. OATs from non-GO patients (n=11) who were free of thyroid or other inflammatory eye disease and were undergoing augmented upper eyelid blepharoplasty surgery. OAT-PFs were obtained from adipose tissue explants and WAT-PFs were obtained by collagenase digest, both as previously described (17). Cells were used at low passage number (<5), hence not all samples were analyzed in all experiments.

Preadipocytes/fibroblasts culture and in vitro adipogenesis

Preadipocytes/fibroblasts (PFs) were cultured in DMEM/F12 10% FCS (complete medium, CM). Adipogenesis was induced in confluent cells by replacing with ADM (adipogenic medium) containing 10% FCS, biotin (33uM), panthothenate (17uM), T3 (1nM), dexamethasone (100nM), thiazolidinedione (1uM) and insulin (500nM) for 17

days. Adipogenesis was assessed by microscopic examination to detect the characteristic morphological changes (cell rounding, accumulation of lipid droplets), acquisition of lipid filled droplets (oil-red-O staining) and transcript measurement of terminal adipogenic marker (lipoprotein lipase, LPL) by QPCR as described previously (17).

For experiments using exogenous fatty acid (FA), a fatty acid mixture (200µM) comprising oleate:palmitate:linoleate (45:30:25%) bound to BSA was added to CM throughout the whole time culture as previous described (25), with/without ADP (Adenosine 5'-dphosphate sodium salt), GDP (Guanosine 5'diphosphate sodium salt), oligomycin (mitochondrial inhibitor) or AICAR (adenosine analog) for 17-19 days. Adipogenesis was analysed by foci of differentiation (groups of cells with lipid droplets), which were counted in ten different fields for each experimental condition as described before (16).

Triglyceride (TAG) extraction from differentiated PFs and iLAB analysis

Confluent PFs were cultured in ADM with/without the supplementation of FA, oleate:palmitate:linoleate (45:30:25%), for 10 days in 24-well plate. Cellular TAG from the differentiated PFs were analysed as previously described (25). In brief, cell lysates were obtained using lysis buffer (1% IGEPAL CA-630, 150 mM NaCl and 50 mM Tris-HCl (pH8.0)) and sonication. Some of the lysates were used for protein quantification using BCA assay (Bio-Rad, DC protein assay kit). The lysates used for TAG analysis were heated at 95°C for 30 minutes and centrifuged at 12,000 g for 10 minutes after cooling. Cellular TAG concentration was measured using enzymatic assay (TAG assay, Instrumentation Laboratory UK) with glycerol standards, and run on an ILAB 650 clinical analyzer (Instrumentation Laboratory UK). The normalised

TAG content per unit protein were obtained using the following calculation: TAG (μM) ÷ protein (mg / ml).

NAD(P)H and ATP measurement

Confluent PFs were cultured in CM or ADM for 4 days and changed to CM before the following experiments. Cell number was counted using Cellometer from Nexcelom. MTS assay was performed (indicating the production of NAD(P)H (26)) using CellTiter 96(R) AQueous One Solution Assay from Promega according to the manufacturer's instructions, 490nm absorbance was measured after 2h incubation and normalised by cell number. Cells were harvested after culture in CM or ADM for 4 days, total cellular ATP (μM) was measured using standard ATP dilutions by luminescent ATP detection assay kit from Abcam according to the manufacturer's instructions. Each condition had four repeats for the above experiments.

Mitochondria number analysis by relative QPCR

DNA was extracted from confluent PFs from OAT-H, OAT-GO or WAT using standard protocol and QPCR was conducted using SYBR Green incorporation measured on a Stratagene MX 3000 as previous described (16). Comparative QPCR was measured and expressed relative to a reference DNA RPL13A for mitochondria DNA cytochrome b (Cytob) detection to determine relative mitochondria number using the primers as follows: RPL13A, forward 5'- CTCAAGGTCGTGCGTCTG-3' and reverse 5'-TGGCTTTCTCTTTCCTCTTCT-3'; Cytob, forward 5'-GCGTCCTTGCCCTATTACTATC-3' and reverse 5'-CTTACTGGTTGTCCTCCGATTC-3' as described before (27).

Flow cytometry analysis

Confluent PFs were cultured in CM (as day 0), and changed to CM or ADM for 4 days. Cells number were counted by Cellometer from Nexcelom, and followed the

procedures using flow cytometry (FACS) (BD FACSCanto II systems) with FACSDiva 6.0 software from Becton Dickinson and Co. (Mountain View, CA) as described before (28). In brief, cells were fixed with 100% methanol and permeabilized with 0.1% PBS-Tween20 for 20 min. Cells were then incubated with 10% normal goat serum/0.3M glycine to block non-specific protein-protein interactions followed by primary antibody of mitochondrial-cytochrome-oxidase (MtCO2) (ab3298 from Abcam (RRID:AB_303683), 1µg/1x10^6 cells) or isotype control antibody (mouse IgG) for 30 min. The secondary antibody used Alexa Fluor 488 anti-mouse IgG (1:500 dilution) for 30 min, and then fluorescence emissions were collected for 10,000 cells by FACS analysis. Flow cytometic intensity of positive MtCO2 staining referenced to negative control was analysed using FlowJo software version 10.0.5 (Tree Star, Inc., Ashland, OR).

Mitochondrial functional assays by Seahorse XFe96 Analyzer

Basal Assay medium and XFe96 consumables were purchased from Agilent Technologies; Draq5 was purchased from Abcam for DNA staining. Oxygen consumption rate (OCR) and extracellular acidification rate (ECAR) were measured with the Seahorse XFe96 (Agilent Technologies) using Mito Stress kit according to the manufacturer instructions as described before (29). Briefly, cells were seeded at 1×10^4 per well in Seahorse plate. 48 h post-seeding, confluent PFs were then transferred into non-buffered Seahorse Assay medium containing 17.5 mM glucose, 1.5 mM sodium pyruvate and 2.5mM of L-Glutamine with 3% FCS. Basal cellular respiration rate was first measured followed by oligomycin A injection (1 µM) to inhibit ATP synthase. Maximal respiration capacity was determined in 3.5 µM FCCP. Finally, non-mitochondrial respiration rate was determined using a combination of rotenone (0.5 µM) and antimycin A (1 µM). Measurements were performed with 3

cycles including 4 min of medium mixing followed by 3 min of measurements. For data normalization, cells were fixed for 20 min with 4% PFA. Cell nuclei were then stained for 1 h with Draq5 (ab108410 from Abcam (RRID:AB_2892715)) 1/10000 diluted in PBS +0.1% Tween-20. Stained cells were then detected with Odyssey Scanner (Li-Cor). Fluorescent intensity per well was used to normalize respiration values per well. The average of the non-mitochondrial respiration measures was then subtracted from each corresponding condition/time-point per well; all similar condition measurements per well were then averaged. On day 0 (48 h post-seeding), PFs from OAT, OAT-GO and WAT (n=4 for each) in CM were measured with 5 repeats of each condition from one 96-well plate; day 4 (or day 7) PFs (n=4) in CM and ADM were measured from two 96-well plates. PFs from WAT (n=4), OAT (n=8) and OAT-GO (n=9) were used, and two sets of independent experiments were performed for OAT (n=4 & 4) and OAT-GO (n=4 & 5), respectively.

Cellular ATP production rates by mitochondria-OXPHOS and glycolysis were calculated using obtained OCR and ECAR from Seahorse analysis, taking into account of the acidification rates due to mitochondrial CO_2 production as described previously (30,31).

Statistics

Results were analysed using Prism 5 (version 5.02), data normality was initially analysed using the Kolmogorov-Smirnov test. To compare groups we used the T-test for variables normally distributed and the Mann Whitney test was used for non-normal distributed data. Differences between groups were analysed using one way ANOVA. We applied Dunnett's multiple comparison post hoc test for multiple comparisons when identifying statistically significant differences. In all cases $p<0.05$ was considered significant. Data are presented as mean±SEM.

For correlation analysis, the percentage increased FA-uptake adipogenesis by GDP and measured OXPHOS-ATP/Glycolysis-ATP of the cells were analysed for Normality using the Kolmogorov-Smirnov test. All the data were normally distributed and correlation was analysed using Pearson's correlation.

Result

Depot-specific mitochondrial-ATP production by PFs from OAT in early adipogenesis

We induced in vitro adipogenesis using ADM (adipogenic medium) with a mixed hormonal-cocktail in normal culture medium (CM) on human primary PFs for 17 days. The differentiated cells displayed cell rounding and accumulation of lipid droplets (triglyceride formation) with positive Oil-Red-O staining and the induction of LPL expression (marker of late adipogenesis) as previously reported (17).

We compared the early stages of adipogenesis, prior to the formation of adipocytes, in confluent PFs from WAT, OAT-H or OAT-GO cultured in CM (non-differentiating) or ADM (differentiating) conditions. We analysed mitochondria numbers by relative QPCR of mitochondrial DNA, cytochrome b (Cytob) to a reference genomic DNA, RPL13A. Figure 1A demonstrates lower (35.3±3.2%) mitochondrial number in OAT-H or OAT-GO, either in CM or ADM-condition on day 4 compared to PFs from WAT. Interestingly, mitochondrial-cytochrome-oxidase (MtCO2) levels were significantly higher (52.8±2.5%) in OAT-H and OAT-GO compared with PFs from WAT using flow cytometry analysis (Figure 1B). MtCO2 is a necessary component of the respiratory chain of mitochondria for OXPHOS-ATP production (32).

Furthermore, we detected a substantially higher production of NAD(P)H (1.23±0.06 fold-increase) indicating increased mitochondrial-OXPHOS activity (MTS assay/10^6 cells (26), Figure 1C) and increased total cellular-ATP (1.97±0.03 fold-increase) of

differentiating-PFs from OAT-H cultured in ADM compared with CM-condition (non-differentiating-PFs) (Figure 1D), which was not observed in WAT. The increased production of NAD(P)H and total cellular-ATP were also observed in differentiating-PFs from OAT-GO compared with non-differentiating-PFs (supplemental Figure S1), however significantly lower fold-increases were observed when compared with OAT-H. There was no significant difference in cell number between PFs cultured in CM and ADM on day 4 (supplemental Figure S2).

Dysfunction of live ATP-production via mitochondrial-OXPHOS in PFs from OAT-GO.

We next explored live ATP-production rates by mitochondrial-OXPHOS or cellular-Glycolysis according to oxygen consumption rate (OCR) and extracellular acidification rate (ECAR) measured by 96-well Seahorse analyser, as previously described (30,31). Analyses were performed at basal-day-0 in CM-condition or on day 4 and 7 in CM & ADM conditions at early adipogenesis, i.e. before observation of any differentiated adipocytes. All the obtained data were referenced to cell DNA staining at each time point and condition.

During early adipogenesis, an increased OXPHOS-ATP level of differentiating-PFs was observed compared to non-differentiating-PFs on day 4 from WAT, OAT-H and OAT-GO, and further increased on day 7 from WAT and OAT-H, but not OAT-GO (Figure 2A). We then looked detail into changes in OXPHOS & Glycolysis-ATP levels in PFs from OAT-H and OAT-GO separately.

From OAT-H, non-differentiating-PFs had substantially decreased Glycolysis-ATP level on day 4 compared with day 0 and day 7 (Figure 2B), accompanied by unchanged levels of OXHPOS-ATP (Figure 2A). Consequently, there was a higher OXPHOS-ATP/Glycolysis-ATP ratio on day 4 compared with day 0 and day 7 in non-

differentiating-PFs (Figure 2C). Interestingly, in differentiating-PFs (through adipogenesis), significantly higher levels (28.8±11.7%; 46.9±15.3%) of OXPHOS-ATP production (Figure 2A) and OXHPOS-ATP/Glycolysis-ATP ratio (56±10.8%; 68.9±23%) (Figure 2C) with unchanged Glycolysis-ATP (Figure 2B) were observed on day 4 or 7 when compared with day 0, respectively.

From OAT-GO, non-differentiating-PFs showed a trend to increased Glycolysis-ATP levels (Figure 2B) contrasting to a sharp and consistent drop (39.7±7.5%; 40.8±10.7%) of OXPHOS-ATP levels (Figure 2A) on day 4 or day 7 when compared with day 0, respectively. Consequently, there was a trend to decreased ratio of OXPHOS-ATP/Glycolysis-ATP on day 4 & 7 compared with day 0 in non-differentiating-PFs (Figure 2C). Through adipogenesis (Differentiating PFs) in OAT-GO, unchanged levels of OXHPOS-ATP/Glycolysis-ATP & its ratio on day 0, 4 & 7 were observed contrasting with our findings in OAT-H (Figure 2).

In summary, there is a reduction in ATP production by OXPHOS in OAT-GO non-differentiating-PFs, which recovers somewhat in differentiating-PFs. By contrast this reduction of OXPHOS-ATP production is absent in healthy OAT non-differentiating-PFs and levels increase as PFs differentiate.

FA-uptake-driven adipogenesis and the link with mitochondrial in OAT

Cells with lipid droplets and positive Oil-Red-O staining were identified as differentiated adipocytes, and a foci count was performed as described before (16).

1) In order to investigate FA-uptake-driven adipogenesis in vitro, we cultured confluent PFs from OAT-H or OAT-GO with extra free FA using a mixture of three major triglyceride FA, oleate:palmitate:linoleate (45:30:25%) as described in the investigation of FA-uptake in PFs from WAT (25). As expected, differentiated adipocytes were apparent in ADM after 17 days full-differentiation protocol with

adipogenesis hormonal-cocktail, while no adipogenesis was observed in CM-condition (Figure 3A). Addition of the FA-supplement to ADM, led to the differentiated adipocytes as early as day 10, which had about 3-fold higher cellular triglyceride per protein unit compared with adipocytes in ADM alone which were still at the early-middle stage of adipogenesis (supplemental Figure S3).

The effect of FA and the role of mitochondria in OAT-adipogenesis were further investigated by culturing confluent PFs from OAT-H and OAT-GO with FA-supplement in CM without adipogenesis hormonal-cocktail and with addition of different concentrations of mitochondrial bio-substrates, ADP (0.05, 0.1, 0.2mM) and GDP (0.1, 0.5, 1mM) for 17 days. To our surprise, we observed differentiated adipocytes by feeding FA only in CM for 17 days to both OAT-H and OAT-GO PFs (OAT-H n=1 and OAT-GO n=4, Figure 3A). This type of FA-uptake-driven adipogenesis was substantially enhanced by 1mM GDP in CM reaching to 7-18% of ADM-hormonal-cocktail induced adipogenesis (Figure 3A). In contrast, no significant changes in the FA-uptake-driven adipogenesis were observed by ADP-supplement in PFs from both OAT-H and OAT-GO (Figure 3A).

2) We then analysed the effect of the optimal 1mM concentration of GDP and FA supplement in FA-uptake-driven adipogenesis in additional samples. We also tested the effect of ADP and chemical adenosine-analogue/inhibitor of mitochondria (AICAR/oligomycin, respectively). The results are summarised in Figure 3B; we observed differentiated adipocytes from OAT-H (n=1 out of 4) and OAT-GO PFs (n=7 out of 8) by feeding FA in CM. Furthermore, substantially increased FA-uptake-driven adipogenesis in PFs from all OAT-H and OAT-GO was observed upon addition of 1mM GDP (Figure 3B). In contrast, addition of the adenosine-analogue AICAR or ADP had no effect on FA-uptake-driven adipogenesis, and the use of

different concentrations of mitochondrial inhibitor, oligomycin, abolished the induced FA-uptake-driven adipogenesis of all PFs from OAT-H and OAT-GO (Figure 3B).

3) We have replicated the effects of GDP, ADP with FA-supplement in CM on OAT-PFs in further experiments (supplemental Figure S4).

In summary, FA-triggered adipogenesis was observed in OAT-H PFs from 4 out of 5 individuals and 8 out of 10 OAT-GO PFs samples from GO patients. In all cases, this was substantially enhanced by addition of GDP-supplement.

Correlation of FA-uptake-driven adipogenesis by GDP with increased OXPHOS/Glycolysis capacity of PFs from OAT-GO

In 6 OAT-GO samples we had data from both seahorse analysis (Figure 2) and FA-induced adipogenesis (Figure 3).The further enhanced FA-uptake-driven adipogenesis by GDP treatment (percentage increase versus FA-feeding only) significantly and positively correlated with the measured OXPHOS-ATP levels ($r = 0.946$, $p = 0.004$) (Figure 4A) and OXPHOS-ATP/Glycolysis-ATP ratio ($r = 0.840$, $p = 0.036$) (Figure 4C), but not with the levels of Glycolysis-ATP ($r = -0.75$, $p = 0.086$) (Figure 4B) in non-differentiating-PFs at basal-day-0. The further enhanced FA-uptake-driven adipogenesis by GDP treatment significantly correlated negatively with the measured Glycolysis-ATP levels ($r = -0.966$, $p = 0.002$) (Figure 4E) and positively with OXPHOS-ATP/Glycolysis-ATP ratio ($r = 0.857$, $p = 0.029$) (Figure 4F), but no significant correlation with levels of OXPHOS-ATP ($r = 0.096$, $p = 0.857$) (figure 4D) in differentiating-PFs on day 4.

Discussion

Our study demonstrated increased cellular ATP-production via mitochondrial-OXPHOS during adipogenesis of PFs from OAT but not WAT. Mitochondrial dysfunction was observed with disrupted levels of OXPHOS-ATP/Glycolysis-ATP

and its ratio in PFs from OAT-GO compared with OAT-H. Furthermore, FA-supplementation was able to trigger in vitro adipogenesis in PFs from both OAT-H and OAT-GO, which was substantially enhanced by addition of GDP and diminished by mitochondrial inhibitor. The enhanced FA-uptake-driven adipogenesis by GDP was significantly and positively correlated with ratios of OXPHOS-ATP/Glycolysis-ATP at basal non-differentiating-PFs or early-adipogenesis of differentiating-PFs from OAT-GO. Taken together, these observations suggested that an essential role of mitochondrial OXPHOS-ATP production and its bio-substrate GDP in the depot-specific FA-uptake-driven adipogenesis of OAT-H and exacerbated in GO by mitochondrial dysfunction.

Our investigation employed a well-established cell model, heterogeneous population (PFs) derived from the entire stromal-vascular fraction of human orbital (OAT) and WAT (10,33). The key findings of this study were confirmed by using more than one independent technique and the observations from our recent ex vivo OAT analysis (11) as discussed below. The low availability of human orbital PFs precludes the use of a model comprising a homogeneous cell type, although this would be preferable.

We and others have described the multi-differentiation MSC potential of adipose tissue derived-PFs (9-11,34). Classically, in vitro adipogenesis is triggered by ADM with a mixed hormonal cocktail to activate key transcriptional factors, e.g. PPAR, CEBP, etc. (35,36), as routinely used in our lab (17). Our current study demonstrated that FA alone were able to induce in vitro adipogenesis in PFs from OAT-H and OAT-GO. This confirms the depot-specific FA-uptake-driven adipogenesis in OAT, which was suggested by ex vivo analysis of human adipose tissue from our recent study (11). Furthermore, we previously demonstrated an abundant expression of the FA-transporter, SLC27A6, with limited FA-synthesis/lipolysis in OAT in GO

386 supporting the excessive FA-uptake-driven adipogenesis in GO (11). Thyroid
387 hormone, PPARγ ligand and cytokines (e.g. TNF or IL6) play important roles in the
388 pathogenesis of GO reviewed in (2), which may also contribute to OAT adipogenesis
389 through its role in the regulation of lipid metabolism via FA transporter (37,38).
390 Further investigation is needed to dissect the important role of the FA transporter
391 system, in the specific context of the MSC phenotype of OAT-PFs, in the FA-uptake-
392 driven adipogenesis in GO (9-11).
393 Our study revealed that inhibition of mitochondrial-OXPHOS by oligomycin abolished
394 the FA-uptake-driven adipogenesis of OAT, which supports the important function of
395 mitochondria in adipogenesis as reported in other fat depots (20,39). However
396 AICAR (adenosine-analog) or ADP, the activator of AMP kinase (AMPK), had no
397 effect on the FA-uptake-driven adipogenesis of OAT thereby eliminating the AMPK-
398 pathway, which plays important roles in other fat depots (40). By contrast, our
399 current study demonstrated that the depot-specific FA-uptake-driven adipogenesis
400 was substantially enhanced by supplementing GDP in PFs from both OAT-H and
401 OAT-GO. The important role of GDP in mitochondrial function and cellular
402 metabolism has been reported in OXPHOS-ATP production (41) or via GTP/GDP
403 exchange (42). Our study suggested that the reduced mitochondrial-OXPHOS
404 results in more available GDP to form a feedback loop to regulate the FA-uptake-
405 driven adipogenesis in OAT.
406 The current study demonstrated that mitochondrial function in OAT-PFs during
407 adipogenesis is linked with an inducible total cellular-ATP production via
408 mitochondrial-OXPHOS. It contrasts with WAT-PFs, or other human stem cells, that
409 have unchanged or even decreased levels of total cellular ATP, apart from increased
410 OXPHOS-ATP through adipogenesis as observed in this study and by others (39,43).

Our investigation observed a depot-specific higher level of mitochondrial cytochrome-C oxidase (32) with low mitochondria number in PFs from OAT compared with WAT suggesting increased mitochondrial activity rather than numbers. Furthermore, in OAT-H, early adipogenesis (days 0-4-7) is accompanied by a U-shaped distribution (high, low, high) of Glycolysis-ATP and unchanged OXPHOS-ATP levels. In contrast, levels of OXPHOS-ATP fell sharply with compensated high level of Glycolysis-ATP from non-differentiating-PFs from OAT-GO indicating sustained mitochondrial dysfunction of PFs in GO.

Our recent study highlighted the key role of enhanced proliferation of PFs synergized with FA-uptake-driven adipogenesis in the hyperplastic expansion of OAT in GO (11). Studies have shown that the Warburg phenotype of proliferating cells is important to have enhanced Glycolysis with suppressed mitochondrial-OXPHOS, however non-proliferating cells display higher OXHPOS-ATP production with inhibited Glycolysis (44,45). Our data clearly demonstrate OXPHOS-ATP levels falling sharply with compensated high-level of Glycolysis-ATP production in non-differentiating-PFs from OAT-GO, which may trigger the proliferation of PFs in GO (44,45). Once proliferation is induced, we see higher levels of OXPHOS-ATP and low levels of Glycolysis-ATP through adipogenesis in differentiating-PFs from OAT-H reported here, which may in turn lead to inhibition of proliferation and drive PFs to differentiate (44,45). This study provides further support in the positive correlation noted between FA-uptake-driven adipogenesis by GDP and the ratios of OXPHOS-ATP/Glycolysis-ATP through adipogenesis of PFs from OAT-GO. We hypothesise that the levels of mitochondrial OXPHOS-ATP and metabolites (GDP) play central roles in triggering PFs proliferation and excessive FA-uptake-driven adipogenesis of OAT in GO. The uncorrected dysfunction of mitochondria in PFs from OAT-GO leads to maintained

levels of low-OXPHOS/high-Glycolysis causing excessive proliferation, and more available GDP promoting FA-uptake-driven adipogenesis in OAT expansion in GO.

The OAT depot-specific cell signalling cascades (13,14) play a central role in the pathogenesis of OAT expansion in GO through the interplay of TSHR/PKA, IGF1R/PI3K/Akt, mTORC1, and the downstream nucleus factor, FOXOs, (7,46-49), which are also important in mitochondrial function (42). More work is needed to clarify how TSHR/IGF1R interfere with mitochondria via GDP and OXPHOS-ATP production in triggering proliferation and FA-uptake-driven adipogenesis of OAT, e.g. via pathological activation of UCP-1 (11), or interference with the adenylate cyclase system of GTP/GDP exchange to allow the activation of GO targeted TSHR/IGF1R (50,51). However, we hypothesise that the resultant mitochondrial dysfunction in association with FA-uptake mechanism drives OAT expansion in GO (summarized in Figure 5).

Ethical approval

Human Adipose Tissue was collected with informed written consent and approved by the South East Wales Research Ethics Committee (30 May 2006) with registry number (06/WSE03/37).

Acknowledgements

The authors thank patients, who provided samples used for this study. The authors thank Dr Katherine Pinnick and Professor Fredrik Karpe from University of Oxford, who supported FA-supplement culture condition and triglyceride measurement for this study.

Author contributions

LZ designed the study, performed experiments, prepared the figures, and drafted the manuscript; PR, SM and DMT supported LZ for Seahorse technique and analysis; SM supported LZ for OXPHOS-ATP/Glycolysis-ATP calculation using OCR/ECAR; MSD, DAR, ASH, DM supported sample collections with ethical approval and obtained consent forms from patients; ART supported LZ for relative QPCR analysis of mitochondria number; LZ, ML, DMT & CMD interpreted data and finalised the manuscript; all authors revised the manuscript and approved the submitted version.

Reference:

1. Bahn RS. Graves' ophthalmopathy. *N Engl J Med*. 2010;362(8):726-738.
2. Taylor PN, Zhang L, Lee RWJ, Muller I, Ezra DG, Dayan CM, Kahaly GJ, Ludgate M. New insights into the pathogenesis and nonsurgical management of Graves orbitopathy. *Nat Rev Endocrinol*. 2020;16(2):104-116.
3. Bahn RS, Dutton CM, Natt N, Joba W, Spitzweg C, Heufelder AE. Thyrotropin receptor expression in Graves' orbital adipose/connective tissues: potential autoantigen in Graves' ophthalmopathy. *J Clin Endocrinol Metab*. 1998;83(3):998-1002.
4. Crisp MS, Lane C, Halliwell M, Wynford-Thomas D, Ludgate M. Thyrotropin receptor transcripts in human adipose tissue. *J Clin Endocrinol Metab*. 1997;82(6):2003-2005.
5. Gerding MN, van der Meer JW, Broenink M, Bakker O, Wiersinga WM, Prummel MF. Association of thyrotrophin receptor antibodies with the clinical features of Graves' ophthalmopathy. *Clin Endocrinol (Oxf)*. 2000;52(3):267-271.
6. Khoo DH, Ho SC, Seah LL, Fong KS, Tai ES, Chee SP, Eng PH, Aw SE, Fok AC. The combination of absent thyroid peroxidase antibodies and high

thyroid-stimulating immunoglobulin levels in Graves' disease identifies a group at markedly increased risk of ophthalmopathy. *Thyroid*. 1999;9(12):1175-1180.

7. Zhang L, Grennan-Jones F, Draman MS, Lane C, Morris D, Dayan CM, Tee AR, Ludgate M. Possible targets for nonimmunosuppressive therapy of Graves' orbitopathy. *J Clin Endocrinol Metab*. 2014;99(7):E1183-1190.

8. Krieger CC, Place RF, Bevilacqua C, Marcus-Samuels B, Abel BS, Skarulis MC, Kahaly GJ, Neumann S, Gershengorn MC. TSH/IGF-1 Receptor Cross Talk in Graves' Ophthalmopathy Pathogenesis. *J Clin Endocrinol Metab*. 2016;101(6):2340-2347.

9. Brandau S, Bruderek K, Hestermann K, Gortz GE, Horstmann M, Mattheis S, Lang S, Eckstein A, Berchner-Pfannschmidt U. Orbital Fibroblasts From Graves' Orbitopathy Patients Share Functional and Immunophenotypic Properties With Mesenchymal Stem/Stromal Cells. *Invest Ophthalmol Vis Sci*. 2015;56(11):6549-6557.

10. Kozdon K, Fitchett C, Rose GE, Ezra DG, Bailly M. Mesenchymal Stem Cell-Like Properties of Orbital Fibroblasts in Graves' Orbitopathy. *Invest Ophthalmol Vis Sci*. 2015;56(10):5743-5750.

11. Zhang L, Evans A, von Ruhland C, Draman MS, Edkins S, Vincent AE, Berlinguer-Palmini R, Rees DA, Haridas AS, Morris D, Tee AR, Ludgate M, Turnbull DM, Karpe F, Dayan CM. Distinctive Features of Orbital Adipose Tissue (OAT) in Graves' Orbitopathy. *Int J Mol Sci*. 2020;21(23).

12. Kumar S, Coenen MJ, Scherer PE, Bahn RS. Evidence for enhanced adipogenesis in the orbits of patients with Graves' ophthalmopathy. *J Clin Endocrinol Metab*. 2004;89(2):930-935.

13. Zhang L, Grennan-Jones F, Lane C, Rees DA, Dayan CM, Ludgate M. Adipose tissue depot-specific differences in the regulation of hyaluronan production of relevance to Graves' orbitopathy. *J Clin Endocrinol Metab*. 2012;97(2):653-662.
14. Zhang L, Ji QH, Ruge F, Lane C, Morris D, Tee AR, Dayan CM, Ludgate M. Reversal of Pathological Features of Graves' Orbitopathy by Activation of Forkhead Transcription Factors, FOXOs. *J Clin Endocrinol Metab*. 2016;101(1):114-122.
15. Smolders MH, Graniewski-Wijnands HS, Meinders AE, Fogteloo AJ, Pijl H, de Keizer RJ. Exophthalmos in obesity. *Ophthalmic Res*. 2004;36(2):78-81.
16. Draman MS, Stechman M, Scott-Coombes D, Dayan CM, Rees DA, Ludgate M, Zhang L. The Role of Thyrotropin Receptor Activation in Adipogenesis and Modulation of Fat Phenotype. *Front Endocrinol (Lausanne)*. 2017;8:83.
17. Zhang L, Baker G, Janus D, Paddon CA, Fuhrer D, Ludgate M. Biological effects of thyrotropin receptor activation on human orbital preadipocytes. *Invest Ophthalmol Vis Sci*. 2006;47(12):5197-5203.
18. Schluter A, Horstmann M, Diaz-Cano S, Plohn S, Stahr K, Mattheis S, Oeverhaus M, Lang S, Flogel U, Berchner-Pfannschmidt U, Eckstein A, Banga JP. Genetic immunization with mouse thyrotrophin hormone receptor plasmid breaks self-tolerance for a murine model of autoimmune thyroid disease and Graves' orbitopathy. *Clin Exp Immunol*. 2018;191(3):255-267.
19. Kazak L, Chouchani ET, Stavrovskaya IG, Lu GZ, Jedrychowski MP, Egan DF, Kumari M, Kong X, Erickson BK, Szpyt J, Rosen ED, Murphy MP, Kristal BS, Gygi SP, Spiegelman BM. UCP1 deficiency causes brown fat respiratory

chain depletion and sensitizes mitochondria to calcium overload-induced dysfunction. *Proc Natl Acad Sci U S A*. 2017;114(30):7981-7986.

20. Sawyer SL, Cheuk-Him Ng A, Innes AM, Wagner JD, Dyment DA, Tetreault M, Care4Rare Canada C, Majewski J, Boycott KM, Screaton RA, Nicholson G. Homozygous mutations in MFN2 cause multiple symmetric lipomatosis associated with neuropathy. *Hum Mol Genet*. 2015;24(18):5109-5114.

21. Combs TP, Pajvani UB, Berg AH, Lin Y, Jelicks LA, Laplante M, Nawrocki AR, Rajala MW, Parlow AF, Cheeseboro L, Ding YY, Russell RG, Lindemann D, Hartley A, Baker GR, Obici S, Deshaies Y, Ludgate M, Rossetti L, Scherer PE. A transgenic mouse with a deletion in the collagenous domain of adiponectin displays elevated circulating adiponectin and improved insulin sensitivity. *Endocrinology*. 2004;145(1):367-383.

22. Kusminski CM, Scherer PE. Mitochondrial dysfunction in white adipose tissue. *Trends Endocrinol Metab*. 2012;23(9):435-443.

23. Bouchez C, Devin A. Mitochondrial Biogenesis and Mitochondrial Reactive Oxygen Species (ROS): A Complex Relationship Regulated by the cAMP/PKA Signaling Pathway. *Cells*. 2019;8(4).

24. Cheng Z, Tseng Y, White MF. Insulin signaling meets mitochondria in metabolism. *Trends Endocrinol Metab*. 2010;21(10):589-598.

25. Todorcevic M, Hilton C, McNeil C, Christodoulides C, Hodson L, Karpe F, Pinnick KE. A cellular model for the investigation of depot specific human adipocyte biology. *Adipocyte*. 2017;6(1):40-55.

26. Berridge MV, Tan AS. Characterization of the cellular reduction of 3-(4,5-dimethylthiazol-2-yl)-2,5-diphenyltetrazolium bromide (MTT): subcellular

556 localization, substrate dependence, and involvement of mitochondrial electron
557 transport in MTT reduction. *Arch Biochem Biophys*. 1993;303(2):474-482.
558 27. Cunningham JT, Rodgers JT, Arlow DH, Vazquez F, Mootha VK, Puigserver
559 P. mTOR controls mitochondrial oxidative function through a YY1-PGC-
560 1alpha transcriptional complex. *Nature*. 2007;450(7170):736-740.
561 28. Draman MS, Grennan-Jones F, Zhang L, Taylor PN, Tun TK, McDermott J,
562 Moriarty P, Morris D, Lane C, Sreenan S, Dayan C, Ludgate M. Effects of
563 prostaglandin F(2alpha) on adipocyte biology relevant to graves' orbitopathy.
564 *Thyroid*. 2013;23(12):1600-1608.
565 29. Russell OM, Fruh I, Rai PK, Marcellin D, Doll T, Reeve A, Germain M, Bastien
566 J, Rygiel KA, Cerino R, Sailer AW, Lako M, Taylor RW, Mueller M,
567 Lightowlers RN, Turnbull DM, Helliwell SB. Preferential amplification of a
568 human mitochondrial DNA deletion in vitro and in vivo. *Sci Rep*.
569 2018;8(1):1799.
570 30. Mavin E, Verdon B, Carrie S, Saint-Criq V, Powell J, Kuttruff CA, Ward C,
571 Garnett JP, Miwa S. Real-time measurement of cellular bioenergetics in fully
572 differentiated human nasal epithelial cells grown at air-liquid-interface. *Am J*
573 *Physiol Lung Cell Mol Physiol*. 2020;318(6):L1158-L1164.
574 31. Mookerjee SA, Brand MD. Measurement and Analysis of Extracellular Acid
575 Production to Determine Glycolytic Rate. *J Vis Exp*. 2015(106):e53464.
576 32. Rak M, Benit P, Chretien D, Bouchereau J, Schiff M, El-Khoury R, Tzagoloff A,
577 Rustin P. Mitochondrial cytochrome c oxidase deficiency. *Clin Sci (Lond)*.
578 2016;130(6):393-407.

579 33. Zuk PA, Zhu M, Ashjian P, De Ugarte DA, Huang JI, Mizuno H, Alfonso ZC,
580 Fraser JK, Benhaim P, Hedrick MH. Human adipose tissue is a source of
581 multipotent stem cells. *Mol Biol Cell*. 2002;13(12):4279-4295.
582 34. Fraser JK, Wulur I, Alfonso Z, Hedrick MH. Fat tissue: an underappreciated
583 source of stem cells for biotechnology. *Trends Biotechnol*. 2006;24(4):150-
584 154.
585 35. Sarjeant K, Stephens JM. Adipogenesis. *Cold Spring Harb Perspect Biol*.
586 2012;4(9):a008417.
587 36. Spiegelman BM, Flier JS. Adipogenesis and obesity: rounding out the big
588 picture. *Cell*. 1996;87(3):377-389.
589 37. Dube E, Gravel A, Martin C, Desparois G, Moussa I, Ethier-Chiasson M,
590 Forest JC, Giguere Y, Masse A, Lafond J. Modulation of fatty acid transport
591 and metabolism by maternal obesity in the human full-term placenta. *Biol*
592 *Reprod*. 2012;87(1):14, 11-11.
593 38. Sinha RA, Singh BK, Yen PM. Direct effects of thyroid hormones on hepatic
594 lipid metabolism. *Nat Rev Endocrinol*. 2018;14(5):259-269.
595 39. Zhang Y, Marsboom G, Toth PT, Rehman J. Mitochondrial respiration
596 regulates adipogenic differentiation of human mesenchymal stem cells. *PLoS*
597 *One*. 2013;8(10):e77077.
598 40. van Dam AD, Kooijman S, Schilperoort M, Rensen PC, Boon MR. Regulation
599 of brown fat by AMP-activated protein kinase. *Trends Mol Med*.
600 2015;21(9):571-579.
601 41. Woyda-Ploszczyca AM, Jarmuszkiewicz W. Different effects of guanine
602 nucleotides (GDP and GTP) on protein-mediated mitochondrial proton leak.
603 *PLoS One*. 2014;9(6):e98969.

42. Demine S, Renard P, Arnould T. Mitochondrial Uncoupling: A Key Controller of Biological Processes in Physiology and Diseases. *Cells*. 2019;8(8).
43. Trayhurn P, Beattie JH. Physiological role of adipose tissue: white adipose tissue as an endocrine and secretory organ. *Proc Nutr Soc*. 2001;60(3):329-339.
44. Harvey A, Caretti G, Moresi V, Renzini A, Adamo S. Interplay between Metabolites and the Epigenome in Regulating Embryonic and Adult Stem Cell Potency and Maintenance. *Stem Cell Reports*. 2019;13(4):573-589.
45. Maldonado EN, Lemasters JJ. ATP/ADP ratio, the missed connection between mitochondria and the Warburg effect. *Mitochondrion*. 2014;19 Pt A:78-84.
46. Chen CC, Jeon SM, Bhaskar PT, Nogueira V, Sundararajan D, Tonic I, Park Y, Hay N. FoxOs inhibit mTORC1 and activate Akt by inducing the expression of Sestrin3 and Rictor. *Dev Cell*. 2010;18(4):592-604.
47. Krieger CC, Neumann S, Place RF, Marcus-Samuels B, Gershengorn MC. Bidirectional TSH and IGF-1 receptor cross talk mediates stimulation of hyaluronan secretion by Graves' disease immunoglobins. *J Clin Endocrinol Metab*. 2015;100(3):1071-1077.
48. Kumar S, Nadeem S, Stan MN, Coenen M, Bahn RS. A stimulatory TSH receptor antibody enhances adipogenesis via phosphoinositide 3-kinase activation in orbital preadipocytes from patients with Graves' ophthalmopathy. *J Mol Endocrinol*. 2011;46(3):155-163.
49. Smith TJ, Kahaly GJ, Ezra DG, Fleming JC, Dailey RA, Tang RA, Harris GJ, Antonelli A, Salvi M, Goldberg RA, Gigantelli JW, Couch SM, Shriver EM, Hayek BR, Hink EM, Woodward RM, Gabriel K, Magni G, Douglas RS.

Teprotumumab for Thyroid-Associated Ophthalmopathy. *N Engl J Med*. 2017;376(18):1748-1761.

50. Johnston CA, Siderovski DP. Receptor-mediated activation of heterotrimeric G-proteins: current structural insights. *Mol Pharmacol*. 2007;72(2):219-230.

51. Schneyer CR, Pineyro MA, Kirkland JL, Gregerman RI. Stimulation of human fat cell adenylate cyclase by GDP and guanosine 5'-O-(2-thiodiphosphate). *J Biol Chem*. 1984;259(11):7038-7044.

52. Harper ME, Seifert EL. Thyroid hormone effects on mitochondrial energetics. *Thyroid*. 2008;18(2):145-156.

53. Le Moli R, Muscia V, Tumminia A, Frittitta L, Buscema M, Palermo F, Sciacca L, Squatrito S, Vigneri R. Type 2 diabetic patients with Graves' disease have more frequent and severe Graves' orbitopathy. *Nutr Metab Cardiovasc Dis*. 2015;25(5):452-457.

54. Starkey K, Heufelder A, Baker G, Joba W, Evans M, Davies S, Ludgate M. Peroxisome proliferator-activated receptor-gamma in thyroid eye disease: contraindication for thiazolidinedione use? *J Clin Endocrinol Metab*. 2003;88(1):55-59.

Supplementary data (4 supplemental figures) 10.6084/m9.figshare.14578311

Figure S1 Fold-increase on day 4 ADM-adipogenesis compared with CM condition.

Figure S2 Cell number count on day 4 adipogenesis.

Figure S3 Increased adipogenesis by FAs supplement in ADM.

Figure S4 Induced adipogenesis by FAs and GDP treatment in CM.

Figure 1. Mitochondria analysis & cellular ATP production of OAT-PFs in ADM-adipogenesis compared with WAT. Confluent PFs from OAT-H, OAT-GO or WAT were cultured in complete medium (CM) or ADM (adipogenic medium) for 4 days. **A**)

DNA extracted from OAT (n=3) & OAT-GO (n=3) or WAT-PFs (n=4) on day-4, relative QPCR of cytochrome b (Cytob, mitochondrial DNA) to RPL13A (reference genomic DNA) was performed. **B**) MtCO2 antibody (mitochondria cytochrome oxidase) was analysed by FACS from confluent OAT (n=4), OAT-GO (n=4) & WAT-PFs (n=7) at day-0 in CM or day-4 in CM & ADM, the percentage of flow cytometic (FL) intensity, positive MtCO2 staining, was shown referenced to negative control. **C**) MTS assay (indicating the production of NAD(P)H and mitochondria-OXPHOS activity (26)) was performed on PFs from OAT-H (n=3) & WAT-PFs (n=4) on day 4 in CM & ADM, 490nm absorbance normalized by cell number. **D**) Total level of cellular ATP (Luminescent ATP detection assay kit) was measured from OAT-H (n=7) & WAT-PFs (n=4) on day 4 in CM & ADM. Histograms = mean±SEM of all samples studied. T-test was used for statistical analysis. ***p≤0.001, ****p<0.0005.

Figure 2. Live ATP production from OXPHOS/Glycolysis in differentiating- or non-differentiating PFs from WAT, OAT-H & OAT-GO. Confluent PFs were cultured in 96-well plates, Oxygen Consumption Rate (OCR) as OXPHOS-ATP and extracellular acidification rate (ECAR) as Glycolysis-ATP were measured using Mito Stress kit from WAT (n=4), OAT (n=8) and OAT-GO (n=9) using Seahorse analyzer. OXPHOS-ATP (**A**), Glycolysis-ATP (**B**) were measured as pmol ATP/min on day (D)0 plate in complete culture medium (CM, white square), or after PFs in CM (non-differentiating) or adipogenic medium (ADM, black square) (differentiating-PFs) for 4 or 7 days and referenced to DNA staining. **C**) Percentage ratio of OXPHOS vs Glycolysis on D0, 4 & 7 with CM or ADM condition were presented. Basal-day-0 levels of ATP production by OXPHOS (4.5 pmol ATP/min), Glycolysis(16.6 pmol ATP/min) and its ratio (31.4%) of PFs from OAT-H were displayed and indicated with dash lines. Histograms = mean±SEM of all samples studied. Data were normally

679 distributed, a one-way ANOVA with Dunnett's multiple comparison test or t-test was
680 used to compared D4 or D7 time points with D0 (^); or t-test was used to compared
681 between CM and ADM on D4 and D7 (*). *p<0.5; **p≤0.01; ***p<0.005; ****p<0.0005.

682 **Figure 3. The link of mitochondrial-OXPHOS in FA-uptake-driven adipogenesis**
683 **of PFs from OAT. A)** Confluent cells from OAT-H (n=1) and OAT-GO (n=4),
684 passage 2-4, were cultured in CM or ADM (black square), or with FA supplement in
685 CM (square with dot) for 17 days with treatment of ADP (0.05mM, 0.1mM or 0.2mM),
686 or GDP (0.1mM, 0.5mM or 1mM); **B)** Confluent cells from OAT-H (n=4, white column)
687 or OAT-GO (n=8, black dot column), passage 2-3 were cultured in CM with FA
688 supplement for 19 days, with/without 10ng/ml oligomycin-A (Olig-10), 100ng/ml
689 oligomycin-A (Olig-100), 0.1mM ADP, 0.1mM AICAR, 1mM GDP. Cells were then
690 fixed and stained using oil-red-O technique. Differentiated adipocytes (with lipid
691 droplets) were observed and counted in ten different fields. Representative photos
692 were shown with arrows indicating differentiation adipocytes (x10 mignification).
693 Histograms = mean±SEM of all samples studied. Normal (t-test) or non-normal
694 (Mann Whitney test) distributed data was analysed accordingly. *p<0.05, ***p<0.005.

695 **Figure 4. Correlations of FA-uptake-driven adipogenesis by GDP treatment**
696 **with levels of OXPHOS/Glycolysis-ATP in PFs from OAT-GO.** The scatterplot
697 showing the relationship between percentage induced FA-uptake-driven
698 adipogenesis by GDP+FA vs FA-only, and levels of **A**) OXPHOS-ATP (dot), **B**)
699 Glycolysis-ATP (triangle) and **C**) the percentage ratio of OXPHOS/Glycolysis (square)
700 in non-differentiating-PFs at basal day 0; or **D**) OXPHOS-ATP levels, **E**) Glycolysis-
701 ATP levels and **F**) the percentage ratio of OXPHOS/Glycolysis of differentiating-PFs
702 on day 4 adipogenesis. Statistically Pearson's correlations for the normally
703 distributed data have shown (significant correlations were underlined).

Figure 5. **The essential role of mitochondrial-OXPHOS for FA uptake-driven adipogenesis in the hyperplastic OAT expansion.** Our study demonstrated a depot specific cellular ATP production via mitochondrial-OXPHOS through adipogenesis in OAT-PFs. Dysfunction of mitochondria (dys-Mt) with disrupted OXPHOS-ATP production was observed in PFs from OAT-GO due to GO factors, e.g. TSHR/IGF1R etc. (11,17,18,21,52-54). **Hypothesis**: Mitochondrial OXPHOS-ATP production through adipogenesis is important in maintaining OAT stability by forming a beneficial relationship with the available GDP in PFs to maintain a healthy (low) level of proliferation/adipogenesis in OAT-H (highlighted in dash blue-square). The pathological fall in OXPHOS-ATP with compensated high-level of Glycolysis-ATP by GO factors triggered the proliferation of PFs in OAT in GO, the kept low-level of mitochondrial-OXPHOS and consequent higher GDP availability drive excessive fatty-acid uptake-driven adipogenesis in OAT in GO (highlighted in red-square). Dashed lines indicate proposed mechanism scheme.

719 **Figure 1**

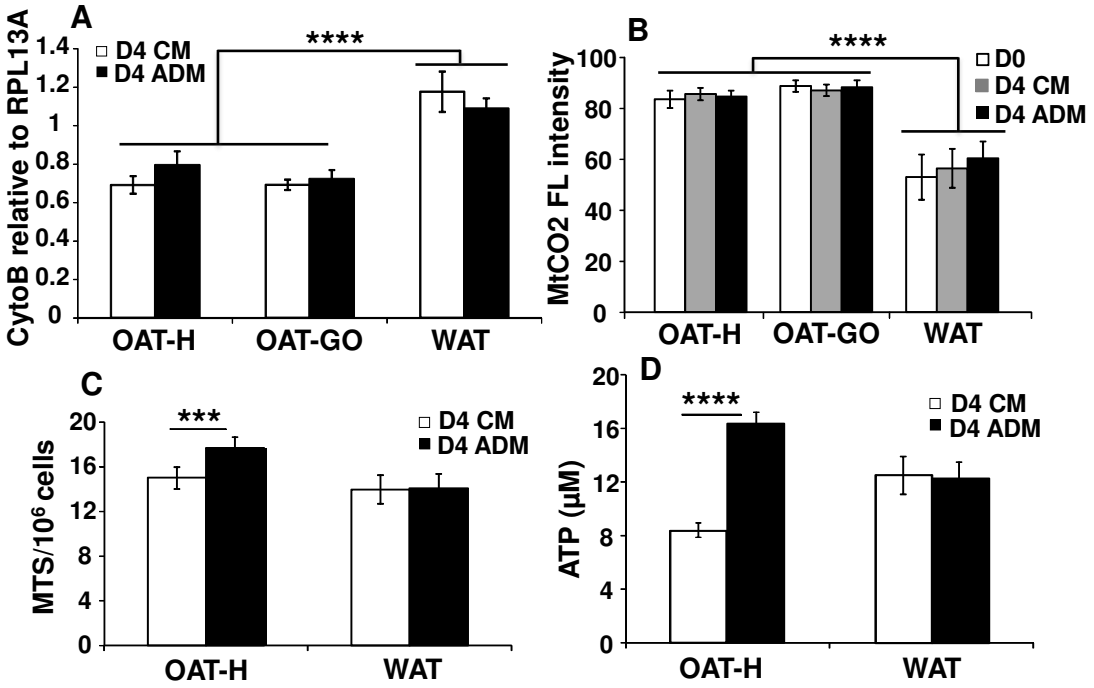

720

721 **Figure 2**

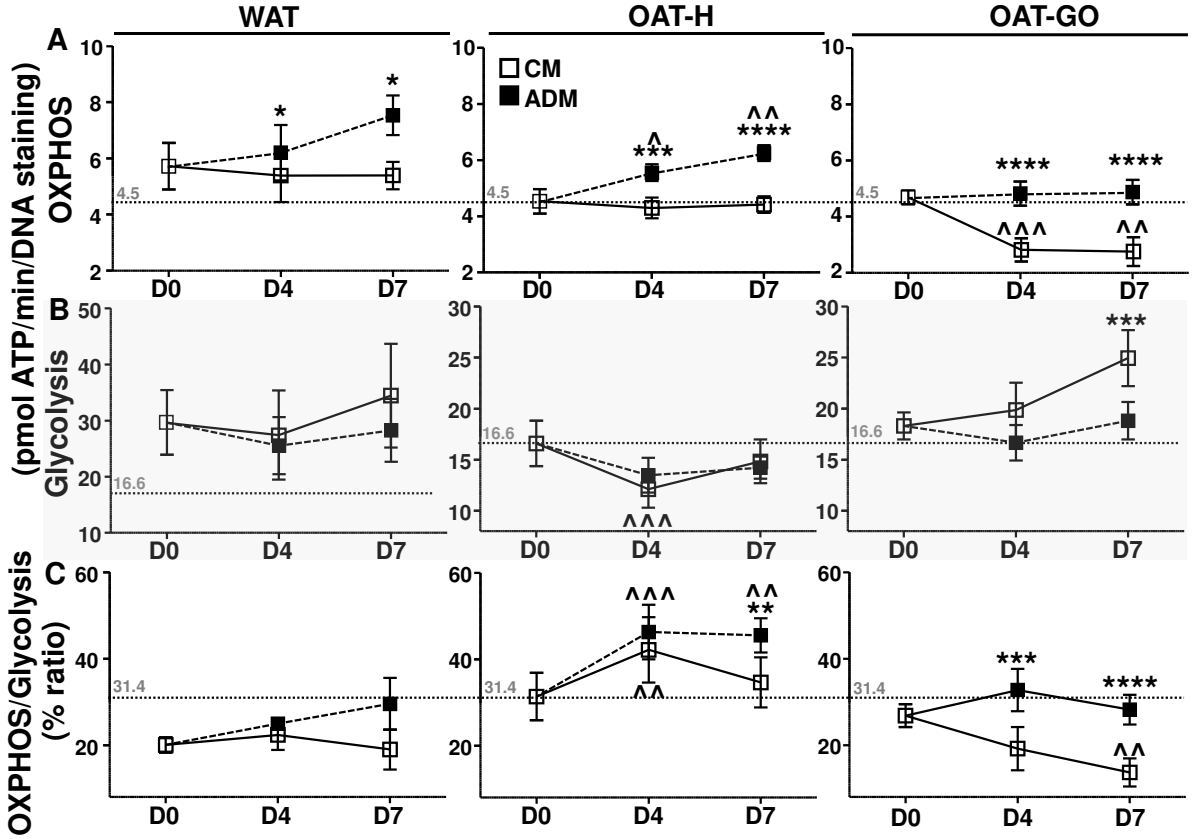

722

723

724 **Figure 3**

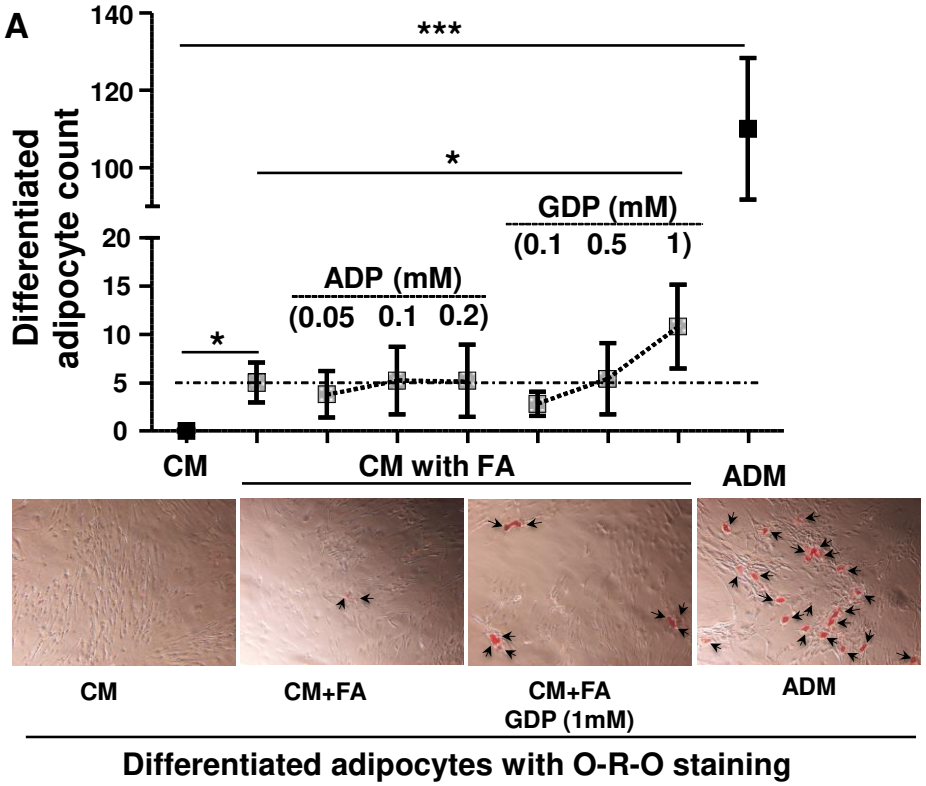

725

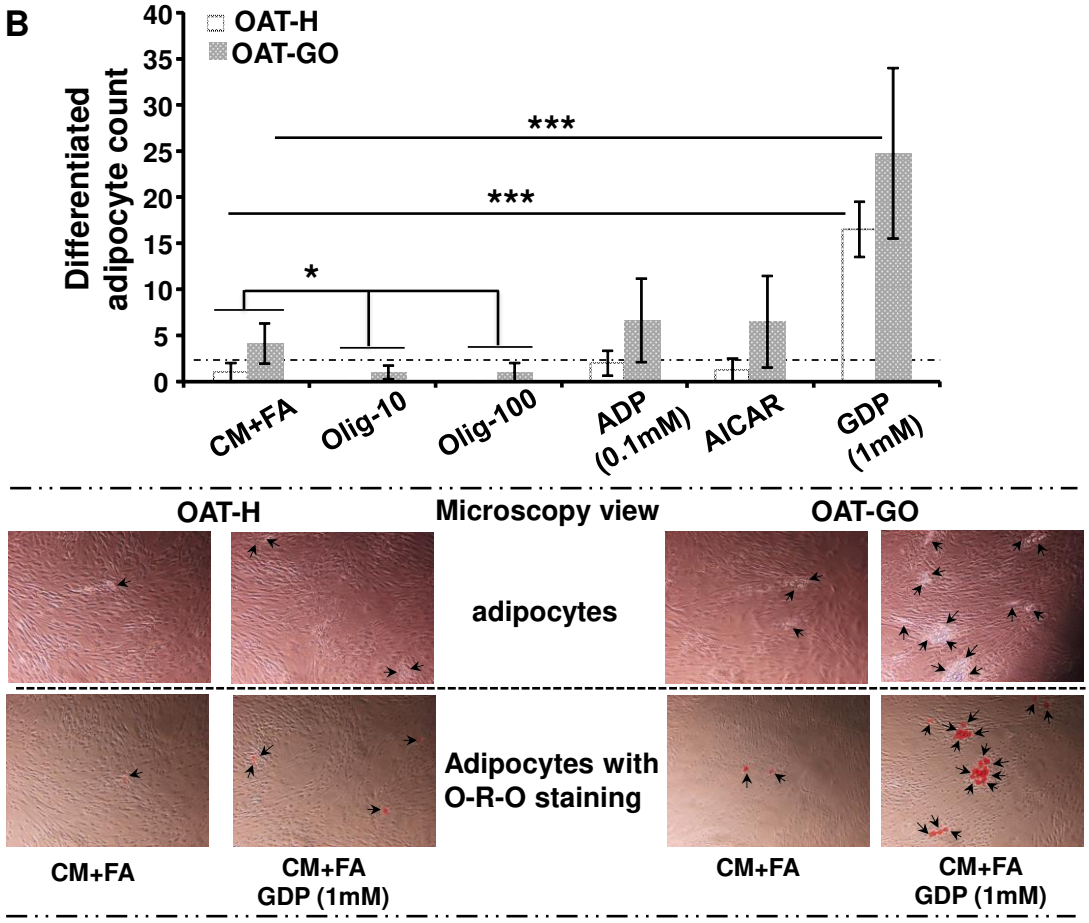

726
727

728 **Figure 4**

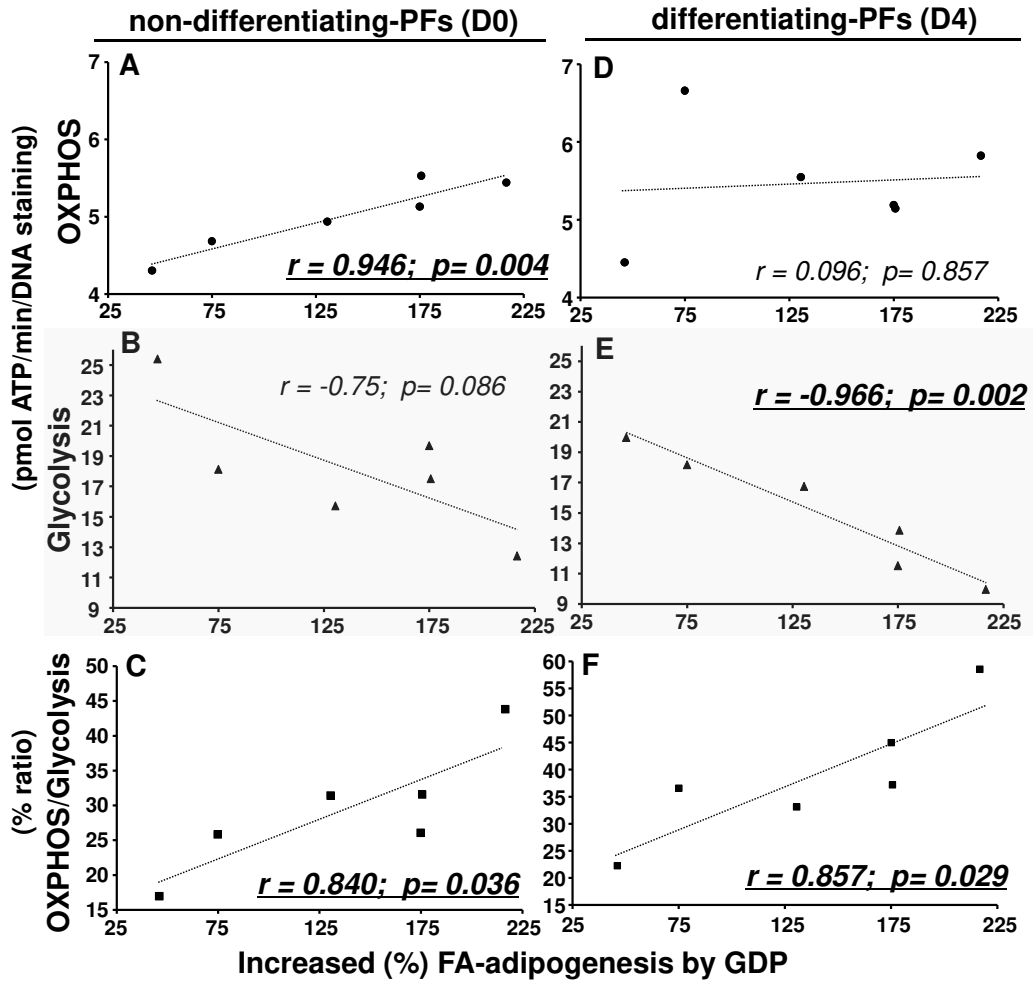

729

730 **Figure 5**

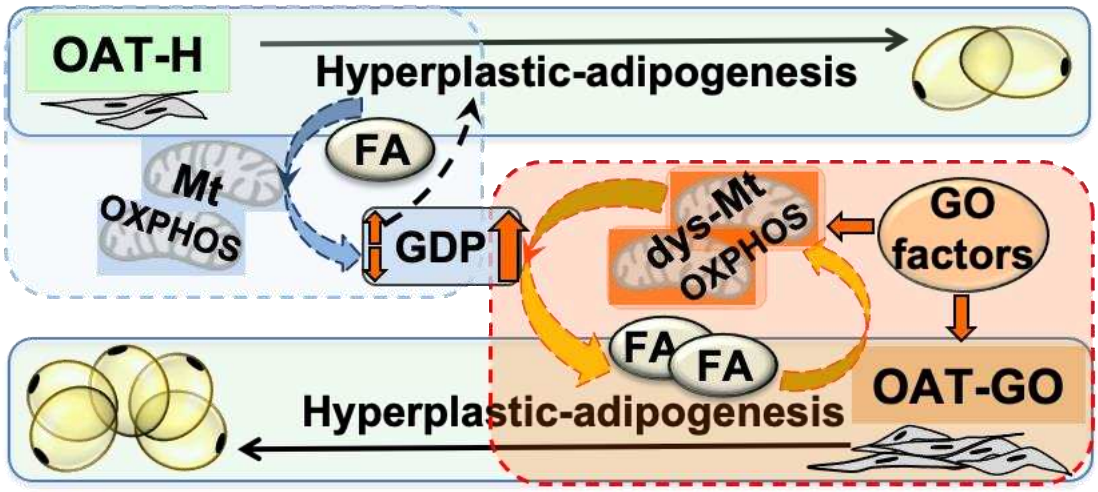

731